17th Brazilian Congress of Thermal Sciences and Engineering
November 25th-28th, 2018, Águas de Lindóia, SP, Brazil

ENCIT 2018 – 0134
MATHEMATICAL MODELING OF A SOLID WASTE INCINERATION SYSTEM AND STEAM GENERATION

Matias Nicolas Muñoz, matiasmunuoz@gmail.com
José Viriato Coelho Vargas, vargasjvcv2@gmail.com
Wellington Balmant, wbalmant@gmail.com
Luiz Fernando Rigatti, eng.rigatti@hotmail.com
Leonardo Martinez, leonardo.cmartinez@live.com
Iago Gomes Costa, iago_gomes_costa@hotmail.com

Graduate Program in Mechanical Engineering (PGMec) and Self-Sustainable Energy Research and Development Center (NPDEAS) Federal University of Paraná (UFPR) – Department of Mechanical Engineering Av. Cel. Francisco H. dos Santos, 100 – Jardim das Américas, Curitiba – PR, 81530-000.

Abstract. *This article presents a mathematical model of an incinerator of urban solid waste and a dimensionless mathematical model of a heat exchanger. The model combines the principles of thermodynamics and heat and mass transfer, assuming thermodynamic control volumes for each component. The mathematical model is explained by a system of ordinary differential equations integrated in time. For the heat exchanger, a dimensionless group of parameters was identified and presented in the form of graphs. The waste incinerator and the heat exchanger are already built and instrumented to obtain real temperature data. Therefore, the model was adjusted from a set of experimental data. Furthermore, the study analyzes the optimization of the distribution of the total area of heat transfer in the heat exchanger. In determining the distribution of the heat transfer area, the phase changes on the cold side of the heat exchanger (overheating, boiling and liquid) must be considered. The results, using wood burning emissions ($CH_{1,44}$ $O_{0,66}$) show that the ideal distribution of the heat transfer area is obtained when the ratio of fluids is Mopt=0.18 the size being determined for the heat exchanger of heat of N = 9.*

Keywords: *Mathematical modeling, Incineration MSW, Heat exchanger, Thermodynamic optimization.*

1. INTRODUCTION

Throughout the world, the increase in population along with the migration of people from rural to urban areas and industrial expansion lead to the generation of large quantities of waste that cause socio-economic and environmental problems. The World Bank report estimates that 1.3 million tons of waste are currently generated per year worldwide; Of which, approximately 30% of the waste is not collected by the municipal services. According to the Organization for Economic Cooperation and Development (OECD), of the collected MSW, 70% is disposed of in landfills, 19% will be reused or recycled and only 11% will be used in the facilities to recover energy. It is expected that by 2025 the amount of waste will increase to 27 million tons per year. (Moya *et al.*, 2017).

The MSW is considered a renewable resource due to its potential to recover energy through processes such as combustion. The yields of municipal biomass increase in significant amounts every year, which makes it capable of producing enormous amounts of energy. Therefore, it is a good option to overcome the energy deficiency that is generated due to the decrease of other natural energy resources. (Cheng and Hu, 2010).

According to Li *et al*., (2017) the LHV of the MSW that is 7.6 MJ/kg, the energy produced by the incineration of the waste is approximately 73.000 MJ/h ± 4.400 MJ/h for a typical incineration chamber. With such energy, production there is great potential for the use of energy in the future.

Waste-to-energy (WTE) technologies are promising technologies, especially for developing countries, to convert waste into a usable form of energy. In the developed world, the thermal treatment of waste is part of its Integrated Solid Waste Management Systems not only to produce other by-products but also to address global warming and climate change. Globally, WTE plays a vital role in the sustainable waste management and the mitigation of environmental problems (Brunner and Rechberger, 2014). These technologies are generally classified as biological treatment technologies and thermal treatment technologies. (Korai *et al.*, 2017).

In the incineration systems, first, the waste is burned directly in the combustion chamber at a suitable temperature (800 - 950 °C) using combustion gases and preheated air. Generally, most of the incinerators have a second combustion chamber in order to guarantee the complete combustion of all the contaminating gases, in this way, to release clean emissions. After the waste incineration process, superheated steam is produced and then it is used within a cogeneration system to produce energy and heat. Electric power is produced by a turbine connected to a generator (Tan *et al.*, 2014).

2. MATHEMATICAL MODEL

In this work, we consider the mathematical model of a solid urban waste treatment plant with energy generation. The physical system considered in Figure 1. In which four control volumes were selected: incinerator composed of two volumes of combustion chamber one (CC-1) and combustion chamber two (CC-2), a heat exchanger and to finalize a water reservoir where it is deposited the superheated steam stream.

For the construction of the equations that describe the behavior of each control volume, was used the technique called volume elements method (VEM). (Vargas and Araki, 2016). On the other hand, to describe the behavior of the heat exchanger was used the NTU efficiency method. (Bejan, 1997).

The first and second thermodynamic laws along with the heat transfer equations were used to characterize the physical system. To simulate the behavior of the system, a code was created using the FORTRAN® 95 software. In this way, we obtain a system of linear and non-linear equations that are solved using numerical methods such as Runge Kutta, bisection, combined secant and Newton Raphson. (Vargas and Araki, 2016).

The mathematical model of the water reservoir and incinerator is developed for the transient regime, while, the heat exchanger operates in the quasi-stationary regime. For that, it is assumed that the thermal inertia of the water tank is much greater than the thermal inertia that the heat exchanger has. (Bejan, 1997).

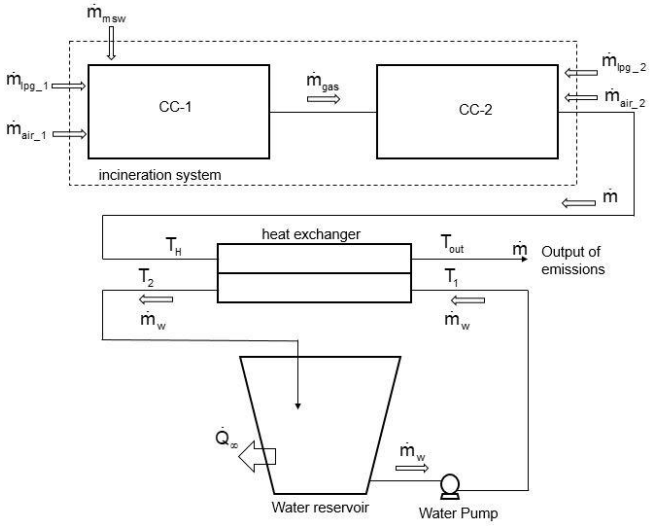

Figure 1. Diagram of the waste heat treatment and steam generation system.

2.1 First combustion chamber

The first combustion chamber of the incinerator is fixed bed and has a mobile grid, in this volume, the almost total combustion of waste is produced. It is rectangular in geometry. It also has a burner system powered by liquefied petroleum gas (LPG) used as an auxiliary fuel to start combustion, on the other hand, it has the air supply system to complete the combustion cycle. All products (MSW, LPG and air) that enter the control volume are considered at room temperature. The mass flow of gas leaving the system is calculated as follows:

$$\dot{m}_{gas\_1} = \dot{m}_{lpg\_1} + \dot{m}_{air\_1} + \dot{m}_{msw} \tag{1}$$

The stoichiometric reaction of combustion, considering the existence of biomass (wood) and LPG gas in the fuel mixture, as follows:

$$x(\xi CH_{1.44}\, O_{0.66}) + y(\alpha C_3H_8 + \beta C_4H_{10}) + \lambda z(O_2 + 3.76\, N_2) \rightarrow bCO_2 + cH_2O + 3.76\lambda z\, N_2 + (\lambda - 1)\, zO_2 \tag{2}$$

where $CH_{1.44}\, O_{0.66}$ represents biomass (Nussbaumer, 2003), ξ the percentage of the amount of biomass that is burned in the first combustion chamber ~ 70% (Markovic *et al.*, 2014). y represents the gas fraction of LPG in the combustion reaction and α the propane fraction contained in the LPG gas, β is the fraction of butane contained in the LPG gas (Moran *et al.*, 2011), balanced coefficients b, c and z in the combustion reaction; and fraction of biomass in the total fuel mixture.

The heat released by the combustion in molar basis is the difference between the specific molar enthalpy of products and reactants, as follows:

$$\bar{Q}_{c\_1} = \bar{h}_{p\_1} - \bar{h}_{r\_1} \tag{3}$$

where $\bar{Q}_{c\_1}$ represents combustion released heat, molar basis, [kJ/kmol] and $\bar{h}_{p\_1}$, $\bar{h}_{r\_1}$ as products and reactants molar enthalpies, [kJ/kmol].

$$Q_{c\_1} = \frac{\bar{Q}_{c\_1}}{M_{fuel\_1}} \tag{4}$$

$$M_{fuel\_1} = x\left[\xi(M_{CH_{1.44}O_{0.66}})\right] + y(\alpha \cdot M_{C_3H_8} + \beta \cdot M_{C_4H_{10}}) \tag{5}$$

Where Q_{c_1} represents heat of combustion, [kJ/kg] and *Mi* as molecular mass of substance *i*, [kg/kmol].

$$\dot{Q}_{c\_1} = \dot{m}_{fuel\_1} \cdot Q_{c\_1} \tag{6}$$

The energy balance in CC-1, considering that the gases behave as an ideal gas, we obtain the temperature in time for this control volume:

$$\frac{dT_{cc\,1}}{dt} = \frac{1}{c_{p,gas}\, m_{gas\_1}} \left\{ \left[\begin{array}{l} \dot{m}_{air\_1} c_{p,air} T_\infty + \dot{m}_{lpg\_1} c_{p,lpg} T_\infty + \\ \dot{m}_{msw} c_{p,msw} T_\infty - \dot{m}_{gas\_1} c_{p,gas} T_{cc\,1} + \dot{Q}_{c\_1} \end{array} \right] - \dot{Q}_1 \right\} \tag{7}$$

The mass flow rates at the CC-1 inlet are at room temperature T_∞ are: air, $\dot{m}_{air\_1}$, LPG $\dot{m}_{lpg\_1}$ and waste $\dot{m}_{msw}$. The total mass resulting from the gases is m_{gas_1}. Where $\dot{Q}_1$ is the heat transfer rate by convection and conduction, and $\dot{Q}_{c\_1}$ is the heat transfer rate by the combustion.

Where, $m_{gas\_1} = \rho_{gas} V_{cc1}$ the gas mass, which is calculated assuming that $\rho_{gas} \sim \rho_{air} = 1{,}225$ kg/m^3 in both chambers, (Moran et al., 2011), with $V_{cc1} = 0.55$ m^3; $c_{p\,gas} = 1{,}005$ J/kg K; $c_{p\,lgp} = 1{,}630$ J/kg K [18, 22], and $c_{p\,msw} = 1{,}354$ J/kg K. (Huron *et al.*, 2017).

The heat transfer system is expressed, as follows:

$$\dot{Q}_1 = U_1 A_1 (T_{cc1} - T_\infty) \tag{8}$$

Where

$$U_1 = \frac{1}{\frac{1}{h_1} + \frac{e_{wall}}{k_{wall}} + \frac{e_{ins\_1}}{k_{ins}}} \tag{9}$$

The $h_1 = 8.4$ W/m^2 K (Kung *et al.*, 1972), coefficient of heat transfer by forced convection inside the combustion chamber; $e_{wall} = 0.005$ m thickness of sheet steel; $e_{ins\_1} = 0.04$ m thickness of thermal insulation (firebrick); $k_{wall} = 43$ W/m K thermal conductivity coefficient and $k_{ins} = 0.1$ W/m K (Bejan, 2013). The heat transfer area is defined $A_1 = 5.10$ m^2.

2.2 Second combustion chamber

The second combustion chamber is a cylindrical reactor sealed hermetically. In this volume, a new combustion of the gases coming from the first chamber occurs and of biomass particles that were not burned in the first combustion. The function of the second chamber is to guarantee the complete combustion of all the products in order to obtain clean emissions. In the reactor has a burner fueled with liquefied petroleum gas (LPG); next to this, there is an air supply system to complete the combustion cycle. The products (LPG and air) that enter the control volume are considered at room temperature. The mass flow of gas leaving the system is calculated as follows:

$$\dot{m} = \dot{m}_{gas\_1} + \dot{m}_{air\_2} + \dot{m}_{lpg\_2} \tag{10}$$

The combustion reaction for the second chamber, considering complete combustion and the existence of biomass and LPG gas in the fuel mixture, as follows:

$$\zeta(\pi CH_{1.44}\, O_{0.66}) + \psi(\alpha C_3 H_8 + \beta C_4 H_{10}) + \lambda z(O_2 + 3.76\, N_2) \rightarrow d\, CO_2 + f\, H_2O + 3.76\lambda z\, N_2 + (\lambda - 1)\, zO_2 \tag{11}$$

The energy balance for second combustion chamber applying the first thermodynamic law and the concept of heat transfer considering the exhaust gases as an ideal gas:

$$\frac{dT_H}{dt} = \frac{1}{c_{p,gas}\, m}\left\{\begin{bmatrix} \dot{m}_{air\_2}\, c_{p,air}\, T_\infty + \dot{m}_{lpg\_2}\, c_{p,lpg}\, T_\infty + \\ \dot{m}_{gas\_1}\, c_{p,gas}\, T_{CC1} - \dot{m} c_{p,gas}\, T_H + \dot{Q}_{c\_2} \end{bmatrix} - \dot{Q}_2\right\} \tag{12}$$

where, $m = \rho_{gas}\, V_{cc2}$ the gas mass, which is calculated assuming that $\rho_{gas} \sim \rho_{air} = 1{,}225$ kg/m^3 in both chambers (Moran *et al.*, 2011), with $V_{cc2} = 0.50$ m^3.

The heat transfer system is expressed as follows (Incropera *et al.*, 1996):

$$\dot{Q}_2 = U_2 A_2 (T_H - T_\infty) \tag{13}$$

Where

$$U_2 = \frac{1}{\frac{1}{h_2} + \frac{e_{wall}}{k_{wall}} + \frac{e_{ins\_2}}{k_{ins}}} \tag{14}$$

The $h_2 = 8.4$ W/m^2 K (Kung *et al.*, 1972), coefficient of heat transfer by forced convection inside the combustion chamber; $e_{wall} = 0.005$ m thickness of sheet steel; $e_{ins\_2} = 0.06$ m thickness of thermal insulation (firebrick); $k_{wall} = 43$ W/m K thermal conductivity coefficient and $k_{ins} = 0.1$ W/m K (Bejan, 2013), the heat transfer area is defined $A_2 = 4.90$ m^2.

2.3 Heat exchanger

Considering a heat exchanger where $\dot{m}$ is the mass flow and T_H the temperature of the exhaust gases that it produces in the thermal treatment of the waste. It seeks to maximize the output power $\dot{W}$ or to minimize the total entropy generation rate of the heat exchanger.

The following analysis describes our search for this optimal relationship.

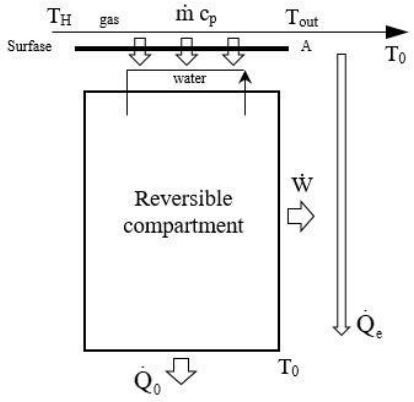

Figure 2. The extraction of power from a stream of hot exhaust.

In this situation, the mass flow, $\dot{m}_w$, is not fixed. The heat transfer from the hot gas to the water stream occurs through a heat transfer surface of area A, which is fixed.

The problem presents several challenges:

First, the water stream can undergo a phase change (vaporization) over an intermediate section of the heat exchanger, where, the temperature of the water remains constant. The second complication is introduced by heat transfer surface A, on the cold side, the heat transfer surface is actually a succession of three sections, the surface, A_w on which the liquid water is heated to the boiling point, the surface A_b on which the current boils and finally, the surface A_s that superheats the steam.

$$A = A_s + A_b + A_w \tag{15}$$

$$\text{Then, } x = \frac{A_s}{A}; y = \frac{A_b}{A}; w = 1 - x - y\frac{A_w}{A} \tag{16}$$

The third complication is the basis of the thermodynamic optimization problem: the flow rate $\dot{m}_w$ is not specified.

The following analysis describes our search for this optimal relationship. We look for the optimal proportion $\dot{m}_w/\dot{m}$ for a given set of constraints (A, U_w, U_b, U_s, T_H, $T_0 = T_\infty$).

The relationship between the flows M to be optimized is defined: $M = \dot{m}_w \big/ \dot{m}$

A- Heat transfer analysis

2.3.1 Superheated section (T_H, T_3, T_b, T_2)

$$N_s = \frac{U_s \cdot x \cdot A}{\dot{m}_w c_{ps}} \cdot \frac{\dot{m} \cdot c_p}{\dot{m} \cdot c_p} = \frac{x \cdot N}{\mu} \tag{17}$$

$$\varepsilon_s = \frac{1 - \exp\left[-N_s (1-\mu)\right]}{1 - \mu \cdot \exp\left[-N_s (1-\mu)\right]} = \frac{\dot{m}_w c_{ps}}{\dot{m}_w c_{ps}} \left(\frac{T_2 - T_b}{T_H - T_b} \right) \tag{18}$$

The capacity rate is $\mu = \dot{m}_w c_{ps} / \dot{m} \cdot c_p$ In this case $Cr = \mu$ therefore:

$$\frac{T_2 - T_b}{T_H - T_b} - 1 = \left[\left(\frac{T_2 - T_b}{T_H - T_b} \right) (\mu - 1) \right] \exp\left[-x \frac{N}{\mu} (1-\mu) \right] \tag{19}$$

$$\text{Then: } \ln\left[\left(\frac{T_2 - T_b}{T_H - T_b} \right) - 1 \Big/ \left(\frac{T_2 - T_b}{T_H - T_b} \right) \cdot (\mu - 1) \right] = x \cdot N \big/ \mu (1-\mu) \tag{20}$$

Finally, the first expression of the system of nonlinear equations to be solved numerically is given by:

$$x = \frac{-\mu \cdot \ln\left[\left(\frac{T_2 - T_b}{T_H - T_b} \right) - 1 \Big/ \left(\frac{T_2 - T_b}{T_H - T_b} \right) \cdot (\mu - 1) \right]}{N \cdot (1-\mu)} = f_1(T_2) \tag{21}$$

2.3.2 Boiling section (T_3, T_4, T_b)

The effectiveness for the boiling section is expressed as follows:

$$N_b = \frac{U_b \cdot A_b}{\dot{m} \cdot c_p} = \frac{U_s \cdot U_b \cdot A \cdot y}{U_s \cdot \dot{m} \cdot c_p} \Rightarrow y = N \frac{U_b}{U_s} \tag{22}$$

Equation (22) is then written as follows:

$$\varepsilon_b = 1 - \exp\left[-y \cdot N \frac{U_b}{U_s} \right] = \frac{\dot{m} c_p}{\dot{m} c_p} \cdot \left(\frac{T_3 - T_4}{T_3 - T_b} \right) \tag{23}$$

The energy balance for the boiling section also states that

$$\dot{m} c_p \, (T_3 - T_4) = \dot{m}_w \, h_{fg} \, (T_b) \tag{24}$$

The following equation is obtained by rearranging the terms of Eq. (24).

$$(T_3 - T_4) = \frac{\mu \cdot h_{fg} \, (T_b)}{c_p T_0 \, (T_3 - T_4)} \tag{25}$$

Equations (24) and (25) deliver

$$1 - \exp\left[-y \cdot N \frac{U_b}{U_s} \right] = \frac{\mu \cdot h_{fg} \, (T_b)}{c_p \cdot T_0 \, (T_3 - T_4)} \tag{26}$$

The second expression of the system of nonlinear equations to be solved numerically is given by

$$y = \frac{1}{N \dfrac{U_b}{U_s}} \ln\left[\frac{\mu \cdot h_{fg} \, (T_b)}{c_p T_0 \, (T_3 - T_4)} \right] = f_2 \, (T_2) \tag{27}$$

2.3.2 Liquid section (T_4, T_{out}, T_b, T_1)

The analysis starts with $\mu' < 1$, using the effectiveness- NTU method as follows:

$$\varepsilon_w = \frac{1 - \exp\left[-N_w \, (1 - \mu) \right]}{1 - \mu \cdot \exp\left[-N_w \, (1 - \mu) \right]} = \frac{\dot{m}_w \, c_{pw}}{\dot{m}_w \, c_{pw}} \left(\frac{T_b - T_1}{T_4 - T_1} \right) \tag{28}$$

Where

$$N_w = \frac{U_s \cdot U_w \cdot A \cdot (1 - x - y)}{U_s \cdot \dot{m} \cdot c_p \cdot \dot{m}_w \cdot c_{pw}} = \frac{U_w}{U_s} (1 - x - y) \frac{\mu}{\mu'} \tag{29}$$

For $Cr = \mu'$, it follows that:

$$\varepsilon_w = \frac{1 - \exp\left[-N_w \, (1 - \mu') \right]}{1 - \mu' \cdot \exp\left[-N_w \, (1 - \mu') \right]} = \left(\frac{T_b - T_1}{T_4 - T_1} \right) \tag{30}$$

Applying ln to Eq. (30), the result is as follows:

$$\ln\left[\frac{\left(\frac{T_b - T_1}{T_4 - T_1}\right) - 1}{\left(\frac{T_b - T_1}{T_4 - T_1}\right)\cdot(\mu' - 1)}\right] = \frac{U_w}{U_s}(1 - x - y)\frac{\mu}{\mu'}(1 - \mu') \tag{31}$$

The third expression of the system of nonlinear equations to be solved numerically is given by

$$(1 - x - y) = \frac{-\mu' \ln\left[\frac{\left(\frac{T_b - T_1}{T_4 - T_1}\right) - 1}{\left(\frac{T_b - T_1}{T_4 - T_1}\right)\cdot(\mu' - 1)}\right]}{\frac{U_w}{U_s} N(1 - \mu')} = f_3(T_2) \tag{32}$$

2.4 Reservoir water

The water reservoir receives heat, that is, the steam that comes out of the heat exchanger. Because the volume of liquid water is much higher in relation to the amount of steam that enters the reservoir, it can be considered that the outlet temperature and the mass of the water in this control volume remains constant and remains that way during all the experiment.

Thus, the mass is obtained as $m_w = \rho_w V_w$, where the volume of water $V_w = 10$ m^3. The density is $\rho_w = 1{,}005$ kg/m^3 and the specific heat of water is $c_{p,w} = 4{,}178$ J/kg K. (Moran *et al.*, 2011). The first law of thermodynamics applied to this system is represented by:

$$\frac{dT_1}{dt} = \frac{1}{c_{p,w} m_w}\left\{\dot{m}_w \left[h(p, T_2) - h_1\right] - \dot{Q}_\infty\right\} \tag{33}$$

The enthalpy of the water at the outlet of the water tank is calculated as $h_1 = c_p T_1$ at atmospheric pressure. However, the water at the entrance of the water reservoir and the outlet of the recovery heat exchanger is superheated steam at T_2 and p = 8 bar Therefore, the enthalpy of superheated steam is calculated by a linear correlation developed from a thermodynamic table of superheated steam (Moran *et al.*, 2011), as follows:

$$h(p, T_2) = 2.1287 \cdot T_2 + 2{,}425.5 \tag{34}$$

The rate of heat transfer between the system and it is the environment is given by (Incropera *et al.*, 1996).

$$\dot{Q}_\infty = U_1 A_1 (T_1 - T_\infty) \tag{35}$$

where, U_1 is the overall heat transfer coefficient across the water box walls, which is defined by a fixed value U_1=100 W/m^2 K. (Bejan, 2013), the heat transfer area was defined in A_1 =51.4 m^2 and the temperature $T\infty$ = 298.15 K.

2.5 System solution

The ten unknowns are, x, y, w, T_3, T_4, T_{out}, T_2, U_s, U_b, U_w, are calculated by the model. The solution to the system of ten equations for a given set of parameters (M, N, T_H, T_b, T_1, U_b/U_s, U_w/U_s) is obtained by combining Eqs. (21), (27) and (32), using the total surface constraint given by Eq. (15), to build the following equation to be solved for T_2 as follows:

$$F(T_2) = f_3(T_2) - \left[1 - f_1(T_2) - f_2(T_2)\right] = 0 \tag{36}$$

Once T_2 is found, the other unknowns for any specific time interval of the quasi-steady simulation are obtained directly by the model.

3. RESULTS AND DISCUSSION

Figure 3 shows the temperature distribution obtained in the simulation of the control volume composed of the first combustion chamber. To simulate the model it is assumed that the mass flow of biomass, air and LPG are fixed and constant over time. The values adopted for the simulations of this study are $\dot{m}_{air\_1} = 0.5\,kg/s; \dot{m}_{air\_2} = 0.1\,kg/s; \dot{m}_{lpg\_1} = 0.0012\,kg/s$ and $\dot{m}_{lpg\_2} = 0.010\,kg/s; \dot{m}_{msw} = 0.021\,kg/s$ .The system has a high airflow and low LPG flow in the first combustion chamber, which was determined to be the best configuration to achieve biomass combustion.

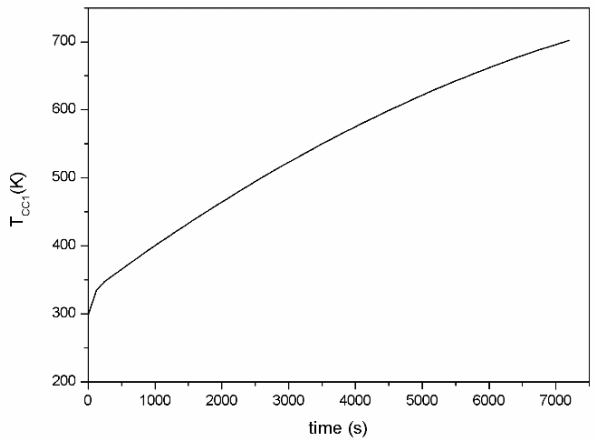

Figure 3. Distribution of temperatures in the first combustion chamber.

Figure 4 shows the distribution of the temperature obtained by the simulation in the second combustion chamber. It is observed that the temperature is approximately 1180 K, compared to the first combustion chamber, this is much higher. Taking into account that the airflow is lower and the injection of LPG is ten times higher in the second chamber than in the first chamber, therefore, you have more fuel to react. In this way, a greater energy is released in combustion. Another observation is that the system enters an almost stationary regime after 2:20 hours of operation.

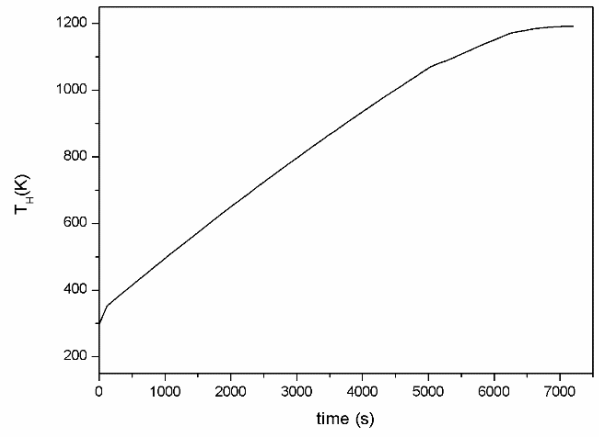

Figure 4. . Distribution of temperatures in the second combustion chamber.

In addition, a factor that contributes to the temperature being higher is that the gases that enter the second chamber do so at a temperature of 700 K. In the analysis of the second chamber, we consider the stoichiometry of the combustion reaction, as well as the heat transfer by conduction and convection.

The Figure 5 show the temperature distribution obtained in the simulation of control volume of the reservoir water.

The steam that is generated by means of the heat exchanger is currently used to heat a body of water contained within a tank. After performing a numerical simulation of 2 hours, the temperature T_1 in the water tank reaches its maximum point at 335 K. In this way, it is verified that the fluid contained in the tank continues to behave like liquid water, given

that the temperature it stays below the boiling point of water. This situation is explained by the fact that the thermal inertia of the water tank is much greater than the thermal inertia of the steam, since the volume of water contained in the tank is much greater than the volume of steam produced.

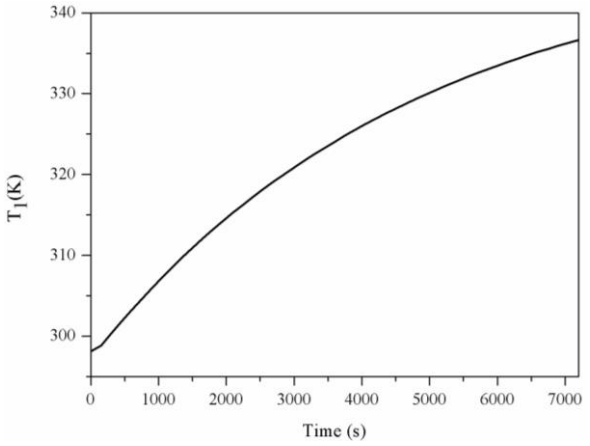

Figure 5. Distribution of temperatures in the reservoir water.

An analysis of the heat exchanger is carried out to determine the temperature distribution of the gases and the fluid inside and outside the control volume. The hot side (gases - emissions), no major complications are observed because the flow is monophasic, while on the cold side (water) the counterflow liquid presents a phase change. Using the NTU efficiencies method, the behavior of temperatures is shown in Fig. 6. The graph is dimensionless for all temperatures, this relationship is $\tau_H = T_H / T_0$.

Figure 6 is made based on the assumption that the global heat transfer coefficient has the same value in each section of the heat exchanger: Us = U_b = U_w. The final temperatures were determined for a water current that enters the exchanger at T_1 = 335 K. The inlet temperature of the gases T_H = 1180 K, considering an ambient temperature of T_0 = 298.15 K and the boiling temperature of T_b = 444.24 K ~ τ_b = 1.49. The exponential shapes of the temperature curve segments are derived from the classical solution for the countercurrent exchanger of the NTU efficiency formulation.

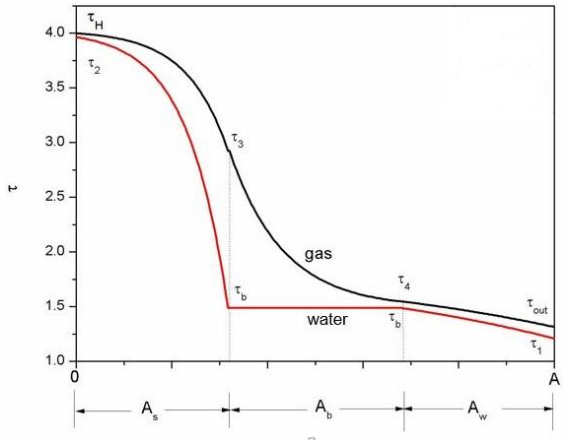

Figure 6. The effect to the heat transfer area size on the match between the temperature distributions of the two streams.

The distribution of the temperature presents was made for a relation of M = 0.18. The water stream has a sudden change in phase when leaving the boiling region; this is due to the difference in temperature from one region to another, which is not very large. On the other hand, between the section of liquid water and boiling the process is slower since the temperature difference between both areas is small.

4. CONCLUSIONS

The conclusion of this study is that the extraction of energy from a hot stream can be maximized by appropriate configurations of the hot stream with a cold fluid receiving stream through a finite-sized heat transfer area. In this study,

a counterflow heat exchanger is used. The proposed results are for a range of M < 1, because it was found that in this situation the system of equations is convergent.

When the cold stream evaporates by capturing a part of the energy of the hot stream, the side corresponding to the cold stream inside the heat exchanger is divided into three sections: liquid preheating, boiling and superheating steam, as shown in Fig. 6 These sections conform to their appropriate relative sizes.

On the other hand, it is possible to obtain the distribution of the temperatures in the combustion chambers taking into account the heat generated in the combustion process by means of an adjustment of the stoichiometric reaction of the biomass. That is, the mathematical model is just right for the performance of the physical model.

5. ACKNOWLEDGEMENTS

The authors acknowledge with gratitude the this research was supported by the National Council for Scientific and Technological Development, CNPq, Brazil, projects 403560 / 2013-6.

6. REFERENCES

Bejan, A. 1997. "*Advanced Engineering Thermodynamics*". 2nd ed. John Wiley & Sons.

Bejan, A. 2013. "*Convection heat transfer*". Fourth ed., John Wiley & Sons.

Brunner, P. and Rechberger, H., 2014. "Waste to energy – key element for sustainable waste management," *Waste Management*, vol. 1, p. 1 – 10.

Cheng, H., Hu, Y. 2010. "Municipal solid waste (MSW) as a renewable source of energy: Current and future practices in China". *Bioresource Technology*. V. 101, pp. 3816-24.

Huron, M., Oukala S., Lardière, J., Giraud N., Dupont C. 2017. "An extensive characterization of various treated waste wood for assessment of suitability with combustion process". *Fuel*. V. 202, pp. 118-128.

Incropera, F.P., DeWitt, D.P., Bergman, T.L., Lavine, A.S. 1996. "*Fundamentals of Heat and Mass Transfer*". John Wiley & Sons.

Korai, M. S., Mahar, R. B., and Uqaili, M. A., 2017. "The feasibility of municipal solid waste for energy generation and its existing management practices in Pakistan," *Renewable and Sustainable Energy Reviews*, vol. 72, p. 338-353.

Kung, H. C. 1972. "A Mathematical Model of Wood Pyrolysis". *Combustion and Flame*. V. 18, pp. 185-195.

Li, C.Y., Wu, J.Y., Zheng, C.Y., Wang, R.Z. 2017. "Effect of LPG addition on a CCHP system based on different biomass-derived gases in cooling and power mode". *Applied Thermal Engineering*. V. 115, pp. 315-325.

Markovic, M., Bramer, E. A., Brem, G. 2014. "Experimental investigation of wood combustion in a fixed bed with hot air". *Waste Management*. V. 34, pp. 49-62.

Moran, M. J., Shapirp, H. N., Boettner, D. D., Bailey, M. B. 2011. "*Fundamentals of engineering thermodynamics*". John Wiley & Sons.

Moya, D, Aldás, C., López, G., and Kaparaju, K., 2017 "Municipal solid waste as a valuable renewable energy resource: a worldwide opportunity of energy recovery by using Waste-To- Energy Technologies" *9th International Conference on Sustainability in Energy and Buildings*, vol. 134, p. 286 – 295.

Nussbaumer, T. 2003. "Combustion and Co-combustion of Biomass: Fundamentals, Technologies, and Primary Measures for Emission Reduction". *Energy & Fuels*. V. 17, pp. 1510-1521.

Tan, S. T., Hashim, H., Lim, J. S., Ho, W. S., Lee, C. T., Yan, J., 2014 "Energy and emissions benefits of renewable energy derived from municipal solid waste: Analysis of a low carbon scenario in Malaysia". *Applied Energy*, vol. 136, p. 797 – 804.

Vargas, J.V.C, Araki, L. K. 2016. "*Applied numerical calculation*". First edition. Manole.

7. RESPONSIBILITY NOTICE

The authors are the only responsible for the printed material included in this paper.